Research article

Ida S. Opstad, Deanna L. Wolfson, Cristina I. Øie and Balpreet S. Ahluwalia*

Multi-color imaging of sub-mitochondrial structures in living cells using structured illumination microscopy

Abstract: The dimensions of mitochondria are close to the diffraction limit of conventional light microscopy techniques, making the complex internal structures of mitochondria unresolvable. In recent years, new fluorescence-based optical imaging techniques have emerged, which allow for optical imaging below the conventional limit, enabling super-resolution (SR). Possibly the most promising SR and diffraction-limited microscopy techniques for live-cell imaging are structured illumination microscopy (SIM) and deconvolution microscopy (DV), respectively. Both SIM and DV are widefield techniques and therefore provide fast-imaging speed as compared to scanning based microscopy techniques. We have exploited the capabilities of three-dimensional (3D) SIM and 3D DV to investigate different sub-mitochondrial structures in living cells: the outer membrane, the inter-membrane space, and the matrix. Using different mitochondrial probes, each of these sub-structures was first investigated individually and then in combination. We describe the challenges associated with simultaneous labeling and SR imaging and the optimized labeling protocol and imaging conditions to obtain simultaneous three-color SR imaging of multiple mitochondrial regions in living cells. To investigate both mitochondrial dynamics and structural details in the same cell, the combined usage of DV for long-term time-lapse imaging and 3D SIM for detailed, selected time point analysis was a useful strategy.

*Corresponding author: Balpreet S. Ahluwalia,** Department of Physics and Technology, UiT-The Arctic University of Norway, Tromsø 9037, Norway, e-mail: balpreet.singh.ahluwalia@uit.no
Ida S. Opstad, Deanna L. Wolfson and Cristina I. Øie: Department of Physics and Technology, UiT-The Arctic University of Norway, Tromsø 9037, Norway

1 Introduction

Mitochondria are indispensable power plants of eukaryotic cells, performing diverse yet interconnected cellular functions. Mitochondrial dysfunction is associated with an increasingly large number of human inherited health disorders that can affect any organ and manifest at any age [1]. The importance of mitochondria and their involvement in many common diseases have made them the target of a vast number of imaging experiments [2–7]. However, despite decades of research, many aspects of their function remain elusive [8–11]. As their function is directly linked to membrane potential and dynamics [12, 13], visualizing these aspects can only be done using live-cell imaging techniques. However, the diameter of mitochondria is typically between 250 and 500 nm. This is quite close to the diffraction limit of conventional visible light microscopy techniques, which is about 200 nm and 500 nm in the lateral and axial directions, respectively. Imaging the complex internal structures of mitochondria using conventional light microscopy would thus be impossible. Their intricate membrane structure has traditionally only been visible through transmission electron microscopy, a method not suitable for live-cell imaging. In recent years, an array of fluorescence-based optical imaging methodologies has emerged, collectively termed super-resolution (SR) optical microscopy or optical nanoscopy [14, 15], which allows imaging beyond the conventional diffraction limit of optical microscopy. However, each technique possesses its own limitations, reducing its capability to rapidly image three-dimensional (3D) samples and similarly limiting its applicability to live-cell imaging [15, 16]. Such limitations include an inability to follow

dynamic processes at the speed dictated by nature, sample motion that can introduce artifacts in the final image reconstruction, or photodamage to delicate structures due to necessarily intense light exposure.

One of the most promising techniques for live-cell SR imaging is structured illumination microscopy (SIM). SIM [17, 18] is a widefield technique that achieves lateral and axial resolution of up to 100 nm and 250 nm, respectively, thus allowing for imaging over a large field of view at relatively high imaging speeds and at low illumination intensities compared to other SR techniques [14, 19, 20]. In addition, SIM is compatible with commonly used fluorescent probes, whereas other SR techniques like single molecule localization methods rely on suitable photoswitchable fluorophores [21], although newer fluctuation-based methods seem promising towards advancing the field in the directions of both live-cell imaging and the use of conventional fluorophores [22, 23]. The resolution doubling provided by SIM, compared to the diffraction limit, is suitable for a coarse determination of sub-mitochondrial structures. Combined with the relatively high imaging speed possible with SIM (0.5–1 Hz), super-resolved time-lapse visualization of live mitochondrial dynamics and even the interplay between different compartments are now possible.

Here, we used 3D SIM and deconvolution microscopy (DV) to simultaneously image three sub-mitochondrial compartments in the same living cell by using spectrally separated probes: mEmerald-TOMM20 (Gtom) for the mitochondrial outer membrane [24, 25], MitoTracker Deep Red (MT) for the mitochondrial intermembrane space, and CellLight Mitochondria-RFP BacMam 2.0 (BM) for the mitochondrial matrix [26, 27]. Each probe has a distinct localization relevant to mitochondrial structure and function. TOMM20 is a subunit of the translocase of the outer mitochondrial membrane complex, which mediates the import of the vast majority of proteins into mitochondria from the cytosol [24, 25]. Inhibition of TOMM20 import has recently been found to play an important role in the pathogenesis of Parkinson's disease [28]. MitoTracker probes accumulate electrophoretically into mitochondria because of their transmembrane potential [29]. Although the permeability of mitochondrial membranes can undergo drastic and rapid changes, MT will normally permeate the mitochondrial outer membrane and accumulate in the intermembrane space near the mitochondrial inner membrane due to its typically low permeability to ions [30]. Finally, BM labels a mitochondrial matrix enzyme (E1 alpha pyruvate dehydrogenase) [26] essential in converting chemical energy from imported nutrients into a usable form for the cell [31]. Deficiency of this enzyme correlates with a buildup of lactic acid and is linked to severe neurological problems [32].

To the best of our knowledge, this is the first report on simultaneously imaging three distinct sub-mitochondrial structures in living cells using optical nanoscopy. Another contribution of this work is to investigate the challenges and opportunities associated with SR imaging and labeling multiple regions inside the same organelle, with an emphasis on mitochondria. Targeting three regions of mitochondria individually was relatively straightforward. However, labeling three sub-mitochondrial regions simultaneously for SR imaging with SIM was found challenging and required re-optimization of the labeling protocols.

2 Results and discussion

2.1 Live imaging of singly labeled mitochondria

To visualize mitochondrial structures, labeling protocols for each probe targeting a sub-mitochondrial structure were optimized on MCC13 cells (Merkel cell carcinoma). For this, we considered factors including label-induced toxicity during both labeling and imaging, the intensity of non-specific background signal, and the photostability of the probe. The optimized protocols are detailed in the methodology section and summarized in Table 1. Briefly, the essential parameters for effective labeling and imaging were as follows: for MT, a working concentration of 75–100 nm and 30-min incubation time and for Gtom and BM, extended post-transfection cell recovery and

Table 1: Overview of necessary re-optimizations for multicolor labeling experiments.

Probe	Optimized labeling
✓ Gtom	1 µg pDNA + 1 µl L3000, 2-day incubation
✓ BM	20 PPT, ~20-h incubation
✓ MT	75–100 nm, 30-min incubation, wash well
Probes combined	Re-optimization
✓ Gtom + BM	Increased time between each transfection (at least 2 days) and higher reagent density of BM (from 20 PPC to 40 PPC)
✓ BM + MT	Increased labeling concentration of MT (400–500 nm)
✓ Gtom + MT	No re-optimization required (individual protocols applicable)
✓ Gtom + BM + MT	Above combined

selection of cells with ideal expression levels for imaging. The sub-mitochondrial localization of each of the three probes evaluated by 3D SIM appeared to be largely in accordance with their expected target regions (Figure 1). For the BM mitochondrial matrix probe, however, larger or thicker aggregates of red fluorescent protein (RFP) were often seen along the mitochondrial network in contrast to their expected appearance as thin, continuous strands (Figure 1A and D). MT, accumulating on the mitochondrial inner membrane, highlighted a folded structure with dark regions or internal gaps, corresponding to the structure of cristae (Figure 1B and E). Gtom, corresponding to the mitochondrial outer membrane, manifested as a wider structure with internal gaps larger than those seen in the other two probes (Figure 1C and F). Supplementary Figure S1 shows a comparison between images obtained using the DV and 3D SIM techniques, where the DV image is mostly unable to reveal the outer membrane localization of the Gtom probe, as clearly shown by the 3D SIM image.

2.2 Time-lapse imaging of mitochondria

Static images cannot provide a complete view of the complex functioning of cellular systems, and an increased interest in mitochondrial dynamics in recent years has resulted in several significant new revelations. Capturing the dynamics of a living system provides a more complete view of its function, with mitochondria being of particular interest recently [33–39]. With this increased interest, however, comes the necessity to better understand how both the labeling and imaging processes themselves may alter the biological system under study and to choose the least invasive technique suited to each study. We attempted 3D SIM time-lapse (TL) imaging of mitochondria labeled as described above, but fast photobleaching hindered capturing dynamics for more than a few frames (typically 1–10).

Interestingly, similar 3D SIM TL experiments on HeLa cells labeled with MTG previously published by Shao et al. [40] did not show the same phototoxicity. They imaged
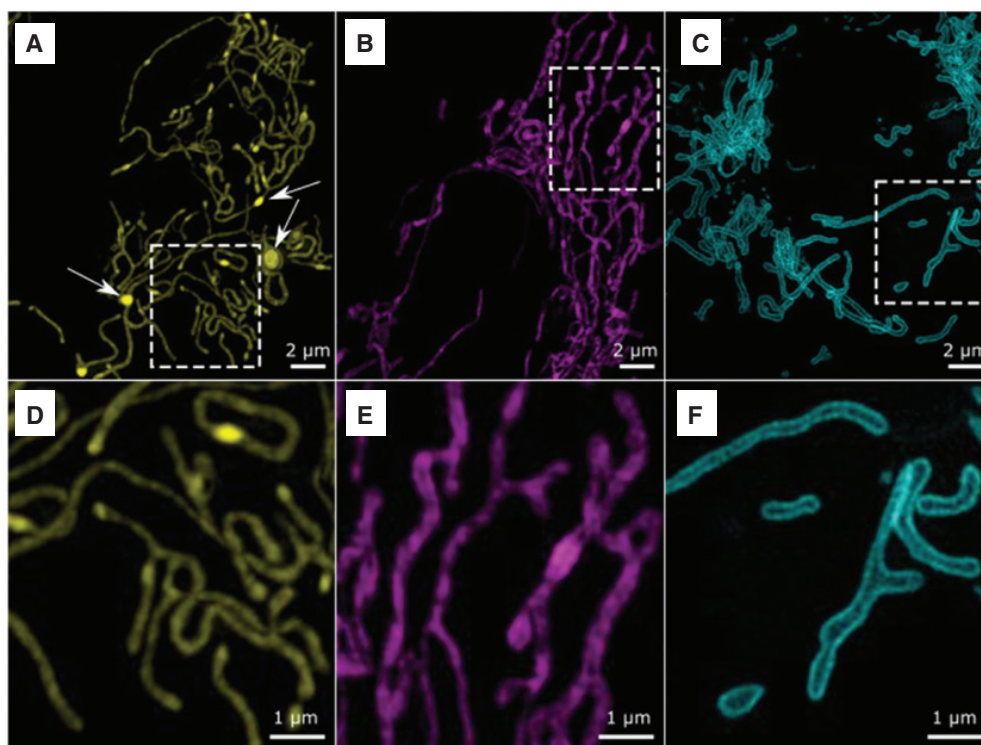

Figure 1: Live imaging of MCC13 cells individually labeled with three mitochondrial probes.
(A) CellLight Mitochondria-RFP BacMam 2.0 (BM) localizes in the mitochondrial matrix. Larger aggregates (indicated by arrows in A) are thought to be labeling artifacts. (B) MitoTracker Deep Red (MT) accumulates in the intermembrane space, and gaps correspond to the presence of cristae. (C) mEmerald-TOMM20 (Gtom) appears along the outer mitochondrial membrane. Panels (D–F) provide a closer look at the boxed regions in A–C. Images are maximum intensity projections of 3D SIM images.
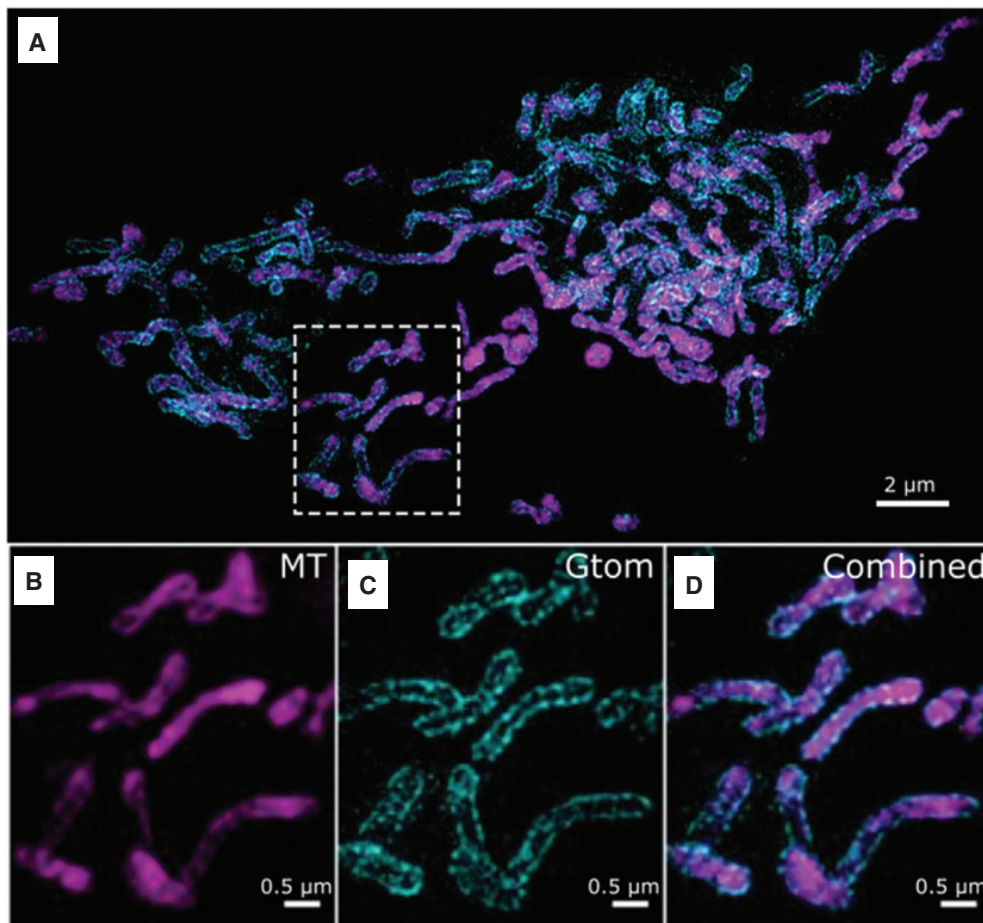
Figure 2: Live imaging of an MCC13 cell dually labeled with Gtom and MT.
The region indicated in (A) is shown magnified below with separate (B, MT; and C, Gtom) and merged color channels (D). Images are maximum intensity projections of a 3-μm 3D SIM z-stack. A single z-slice image with orthogonal views are found in Supplemental Figure S2.

50 time-points seemingly without major morphological artifacts or detrimental photobleaching. Compared to our methods, they imaged approximately double the thickness (6.1 μm) and used half the labeling concentration of MTG (50 nM). The difference may be due to the different cell types used, as HeLa cells are known to be remarkably durable, due to lower label concentration or likely lower illumination intensities, as their exposure time (35 ms) is longer compared to our study (3–8 ms for 100-nM labeling concentration, depending on the brightness of the cell imaged). In our case, however, relatively longer exposure times and lower illumination intensities were not suitable because of the high motility of mitochondria in the chosen cell line (MCC13) and relative intensity of the MitoTracker.

DV, on the other hand, enabled long-term time-lapse imaging (60 time points over 30 min) of all probes. For extended discussion of TL imaging and details on the SIM and DV imaging techniques, see Supplementary note 1: time-lapse imaging, and supplementary movie S1–S2.

As both 3D SIM and DV imaging modalities are available on our microscope, we were able to retain the ability to resolve sub-mitochondrial structures at selected time points by supplementing the DV TL images with 3D SIM images of the same cells. Supplementary Movies S3 and S4 (online material) show 3D renderings of data collected in this way, i.e. a single SIM image and a DV TL series of a Gtom-labeled MCC13 cell, respectively. The 3D SIM image (Supplementary Movie S3) was acquired as the first time point, with the DV TL sequence (Supplementary Movie S4) subsequently acquired after changing the imaging mode on the microscope. This multimodal approach enabled us to balance the need for speed and low light exposure with the desire for SR structural details.

2.3 Live imaging of dually labeled mitochondria

To confirm the sub-mitochondrial localization of the individual probes and their relative colocalization, we labeled the same cells with different live-cell mitochondrial probes. Combining mitochondrial labels in the same sample resulted in reduced labeling efficiency for both BM when following Gtom transfection and for MT following BM transduction (see Supplementary Figure S3). However, no such challenges were encountered for MT labeling following Gtom transfection. The reduced labeling efficiency of dually labeled mitochondria (Gtom + BM and BM + MT) limits the applicability for SIM imaging, as SIM requires a high number of frames with sufficient signal-to-background ratios in order to reconstruct a 3D SIM image. Low fluorophore density, as observed with some of the dually labeled samples, frequently results in rapid photobleaching, reduced image quality, and/or image reconstruction failure while imaging using 3D SIM. Re-optimization of the labeling protocol was therefore necessary for 3D SIM imaging of dually labeled mitochondria, the results of which are summarized in Table 1 and discussed below for different label combinations.

2.3.1 Imaging the mitochondrial outer membrane and intermembrane space (Gtom and MT)

MCC13 cells were first transfected with Gtom and thereafter labeled with MT. As MT resulted in reduced cell health after just a few hours of labeling, transfections, which require long incubation times (e.g. Gtom, see Methods), must be performed first. Figure 2 shows live 3D SIM images of mitochondria dually labeled with Gtom and MT probes. Figure 2B shows MT labeling of the intermembrane space, while Figure 2C shows Gtom labeling of the outer mitochondrial membrane. The resolution provided by 3D SIM is sufficient here to clearly distinguish between the two sub-mitochondrial structures. Supplementary Figure S2 shows a single z-slice image and orthogonal views of this same cell. No additional labeling protocol optimization was necessary beyond that which was used for the probes individually.

2.3.2 Imaging the mitochondrial outer membrane and matrix (Gtom and BM)

Both Gtom and BM labelings rely on the expression of genetically encoded fluorescent fusion constructs – a relatively

slow process. However, the transient nature of BM labeling combined with the necessary cell recovery and expression times thus required Gtom transfection to be performed before BM transduction.

Gtom transfection must be performed at least 48 h before imaging, while for the BM label, a shorter post-transfection incubation time is needed (16–20 h). This makes it tempting to add the BM reagent to the cells about 30 h post-Gtom transfection and thereby (in theory) enabling dual-imaging of both Gtom and BM after 2 days. Based on our experience, however, we do not recommend this approach, as it resulted in a very high cell death rate. Extending the time between the transduction to 2 days resulted in bright dual-labeling of few cells (about 5%), but for the highest possible dual-color labeling efficiency, it was preferable to first induce and maintain a stably transfected cell-line expressing the Gtom label by using antibiotic selection. Without this selection, the Gtom label was gradually lost within a few days post-transfection, thus making dual-labeling extremely unlikely. Under these conditions, many of the dually transfected cells displayed sufficient expression levels of both Gtom and BM for 3D SIM imaging. In Figure 3, 3D SIM images of a Gtom- and BM-labeled cell clearly show the Gtom signal enclosing the BM signal, as expected from their respective localizations on the mitochondrial outer membrane and matrix. Although Gtom labeling negatively impacted BM expression levels, it also appeared to reduce the incidence of morphological artifacts that were observed in cells labeled only with BM, i.e. large aggregates of RFP (shown and further discussed in Supplementary Figure S4).

2.3.3 Imaging the mitochondrial matrix and intermembrane space (BM and MT)

As BM tags an essential mitochondrial metabolic enzyme with a large fluorescent protein, the functioning of the enzyme itself, and thus the mitochondria, may be impacted. Indeed, we observed a reduced labeling efficiency for MT in cells expressing higher levels of BM, such that dual-color imaging was, for most cells, not possible using the same labeling concentration as optimized for MT alone (100 nм) (see Supplementary note 1: time-lapse imaging). However, within the same cultures, we found that some cells with lower expression levels of BM did retain sufficient (though reduced) levels of MT for dual-color SIM imaging, as shown in Figure 4. As higher signal-to-background ratios are needed for successful SIM reconstructions, the cells with higher BM expression
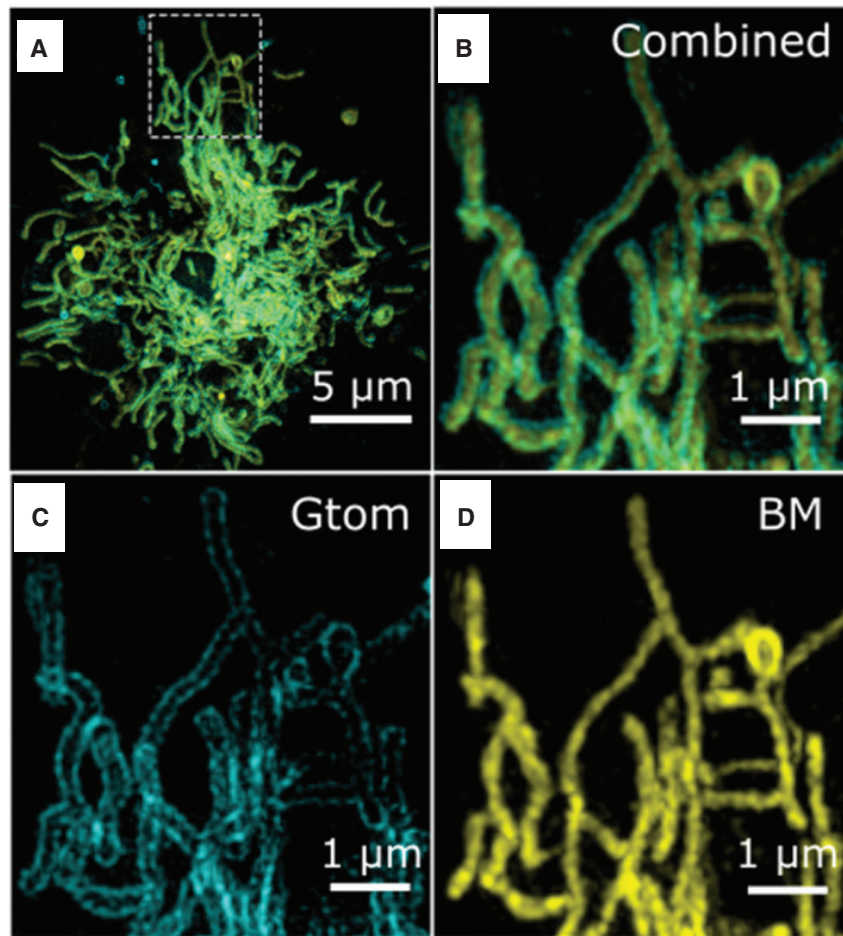
Figure 3: Live imaging of an MCC13 cell dually labeled with Gtom and BM.
The boxed region in (A) is shown magnified for the combined (B) and individual probes (C and D). Gtom (C) localizes at the mitochondrial outer membrane, and the BM label (D) localizes in the mitochondrial matrix. Gtom surrounding BM is shown in the merged image (B). Images are maximum intensity projections of a 1.25-μm 3D SIM z-stack.

levels (and thus higher signal) are better suited for imaging. To compensate for the reduced efficiency of MT labeling on cells showing higher BM expression, MT concentration was increased from 100 nM (the optimized concentration without BM) to 400–500 nM. Increasing the MT labeling concentration above 500 nM induced wider and irregular mitochondrial morphology, together with loss of label specificity, and hence, also poor image quality.

Although moderate increase in labeling concentration provided sufficient signal for dual-color 3D SIM imaging in a greater proportion of the BM-transduced cells, the cells with highest expression levels of BM still did not retain sufficient MT for SIM imaging. Supplementary Figure S5 online shows a SIM image of mitochondria brightly labeled with both BM and MT,

but many, with irregular or ring-shaped morphology. Furthermore, there appear to be very few differences between the BM and MT labels, as mitochondria appear as thin, fairly continuous strings with highly co-localized signals from both labels. It is not clear from these results if the labels are then localized in the mitochondrial intermembrane space or the mitochondrial matrix. This may be due either to the limitation of the resolution that is obtained by 3D SIM compared to the actual dimensions of the mitochondrial compartments or to a possible change in the fluorescent label localization, e.g. the MT label possibly localizing instead in the mitochondrial matrix. The duplication of information from this joint BM-MT approach therefore indicates that its use is limited outside extreme cases of sub-mitochondrial morphological disruption.
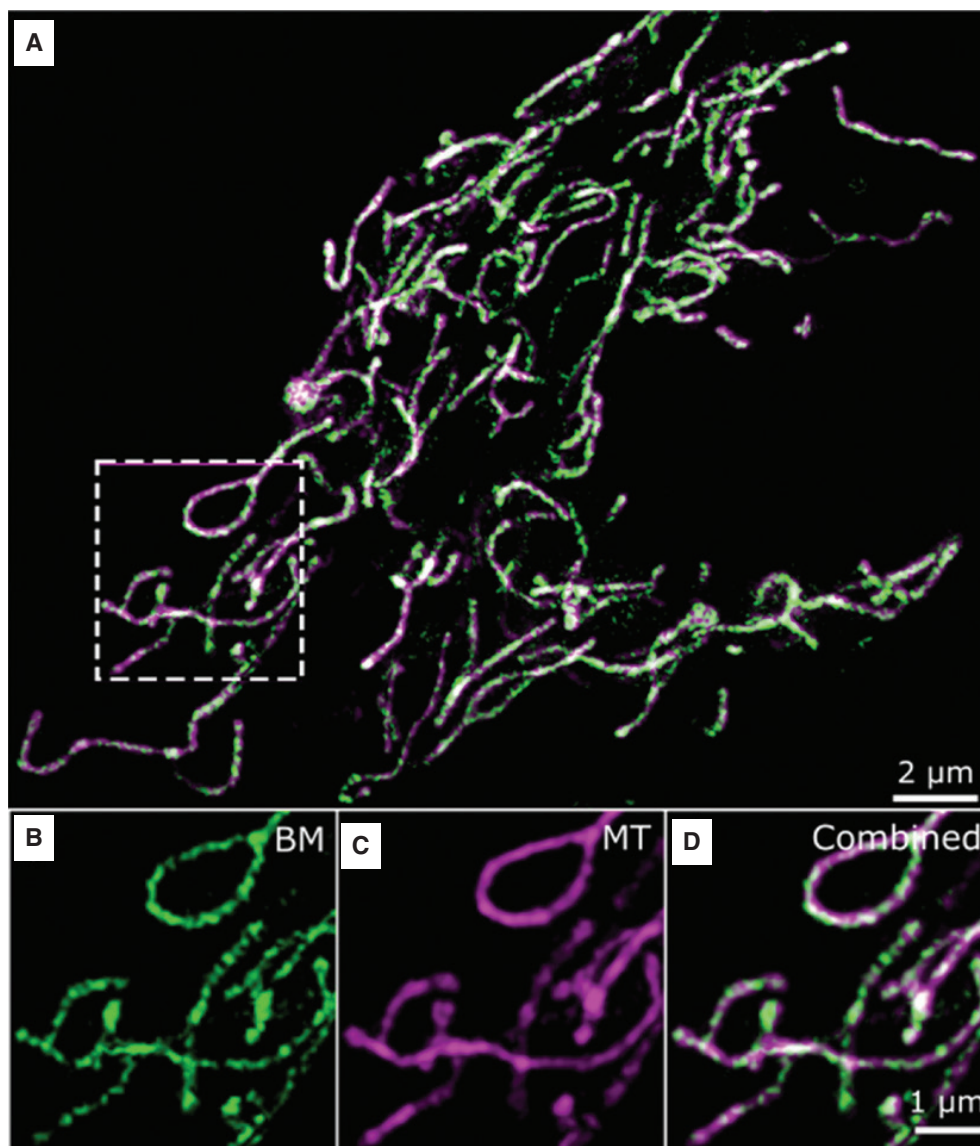
Figure 4: Live imaging of an MCC13 cell dually labeled with BM and MT.
The boxed region in (A) is shown magnified for the individual (B and C) and combined probes (D). For cells with low levels of BM expression, the same concentration of MT could be used as was optimized in MT-alone experiments (100 nм), but the low BM signal compromises image quality (B). Sub-mitochondrial localization cannot be determined in these samples, as the structure of cristae (which had been observable using MT alone) are no longer discernable in the MT channel (C). Images are maximum intensity projections of a 1-μm 3D SIM z-stack.

2.4 Live imaging of triply labeled mitochondria

Using 3D SIM, we imaged mitochondria in living MCC13 cells simultaneously labeled with three spectrally separated probes targeting different mitochondrial structures (outer membrane, intermembrane space, and matrix). Simultaneous labeling with the three probes required overcoming the challenges of combining both Gtom with BM and BM with MT, as discussed in detail in the previous section and summarized in Table 1 and Figure 7. Briefly, this included extending the post-transfection recovery time and increasing the concentration of MT. Additional challenges and optimizations necessary concerning the technical side of multicolor live-cell 3D SIM imaging are discussed below under Imaging conditions.
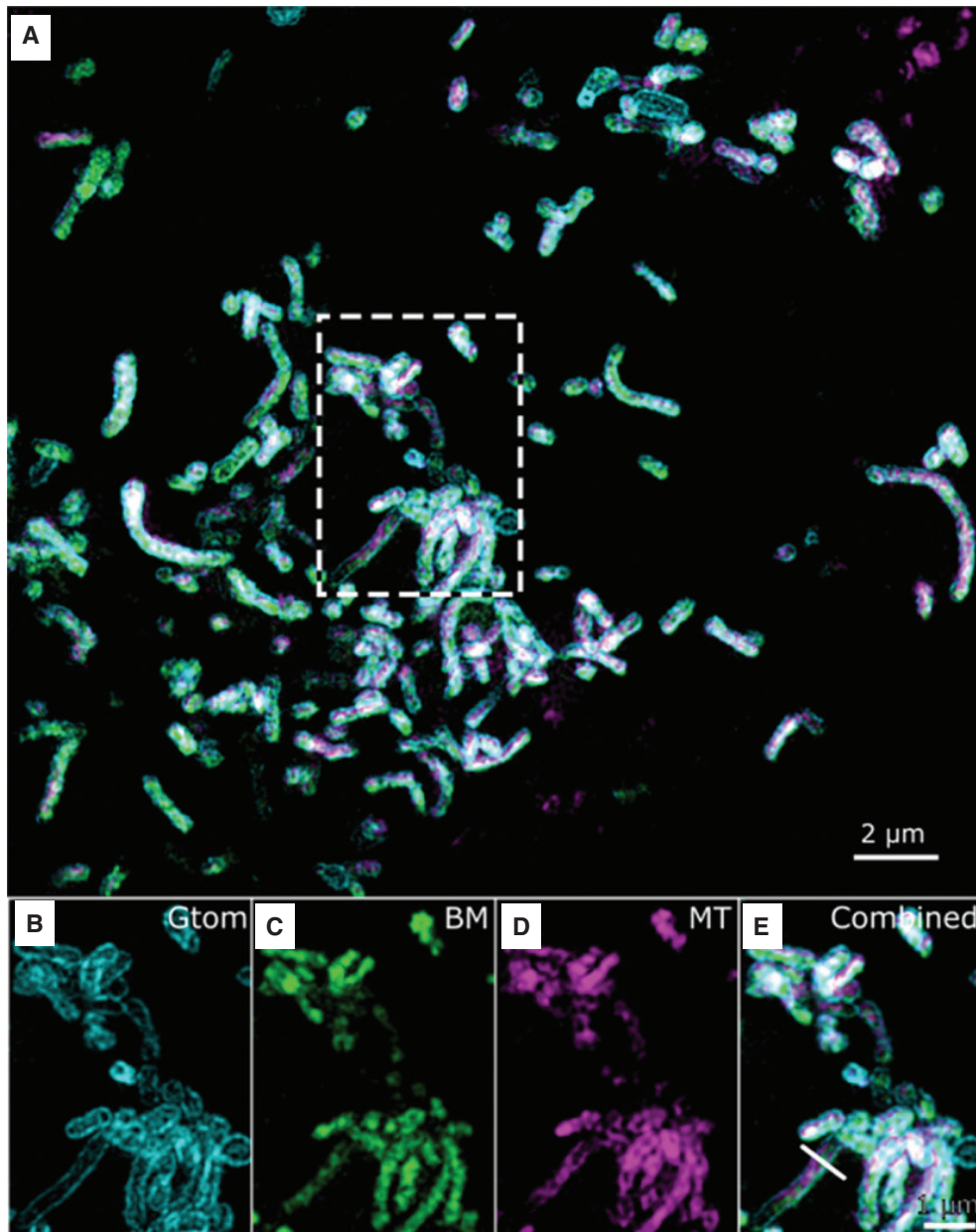
Figure 5: Live imaging of MCC13 cells triple labeled with Gtom, BM, and MT.
The indicated region in (A) is shown magnified below with separate (B) Gtom, (C) BM, (D) MT, and (E) merged color channels. Images are maximum intensity projections of a 1-μm 3D SIM z-stack. The line profile indicated in (E) is plotted in Figure 6, and Fourier plots with resolution estimates of these 3D SIM images are found in Supplemental Figure S8.

Figure 5 shows imaging of the three labeled sub-mitochondrial structures in a single living cell. The localization of the mitochondrial labels was in accordance with both the literature and our results from single-color labeling. BM labeling (mitochondrial matrix) had the slimmest appearance (Figure 5C), while MT (mitochondrial intermembrane space) had a slightly wider appearance and showed discernable gaps or dark regions that corresponded to the inner membrane enveloping the mitochondrial matrix (Figure 5D). Gtom expression (outer mitochondrial membrane) resulted in wider structures (Figure 5B), which clearly enveloped the other two labels (Figure 5E). This enveloping relationship is further demonstrated in a line profile (Figure 6) of the mitochondrion
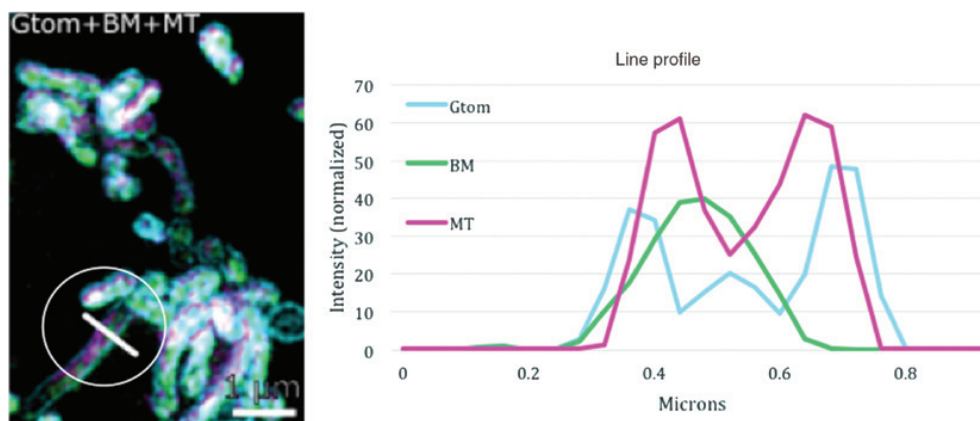
Figure 6: Cross-section of a triply labeled mitochondrion as indicated in Figure 5E and on the left panel.
The plotted intensities have been normalized to the maximum intensity of each individual color channel. Here, BM shows a single peak contained amid the double peaks formed by both MT and Gtom. The width (FWHM) of the blue peaks is around 120 nm, reflecting the expected lateral resolution of the green channel (ex. 488 nm).

indicated in Figure 5E. A single z-slice image of a cell subjected to the same labeling conditions is found in Supplementary Figure S6. Fourier plots estimating the optical resolution are discussed in the Supplementary note and shown in Supplementary Figure S8.

Notably, we found that cells containing sufficient levels of all three probes were less prone to the BM overexpression artifact found in cells labeled only by BM (Supplementary Figure S3). An explanation for this might be that labeling the import protein TOMM20 (in the TOM complex on the outer mitochondrial membrane) may, to some extent, inhibit the import of the BM-fusion protein into the mitochondria. As the cells would thus express a lower and therefore more moderate level of BM, they may be less prone to reduction in mitochondrial transmembrane potential observed in cells with high expression levels of BM. In addition, the successful retention of the MT probe by these cells indicates that the cells were healthier and more viable, with more functional mitochondria.

2.5 Imaging conditions

In addition to optimization of the labeling protocol for live, multicolor 3D SIM of mitochondria, it is also necessary to carefully choose optimal imaging parameters in order to successfully obtain a super-resolved image. The additional light exposure of multicolor imaging increases photobleaching, and when combined with the reduced labeling density (compared to singly labeled samples), it results in an overall decrease in signal intensity. To reduce photodamage [41, 42], lower laser intensities are often used and exposure times increased if higher signal is needed for reliable image reconstruction, although this may also increase motion blur.

Moreover, the SIM reconstruction algorithm for our system assumes a specific point spread function (PSF) for the instrument, yet this PSF is a variable dependent on imaging conditions such as wavelength, temperature, mounting medium, distance from the coverslip, and coverslip thickness. If the PSF used in the reconstruction algorithm does not match the PSF for the particular experimental conditions, image reconstruction may fail or lead to significant artifacts. As it is not practical to measure new system PSFs for each sample, a set of premeasured PSFs is used, with one PSF optimized for each wavelength under standard conditions. One way to compensate for other experimental differences is to change the index of refraction (RI) of the immersion oil used on the objective. Choosing the correct immersion oil for assessment of dual or triple staining of mitochondria in live cells was almost as essential as choosing the correct excitation wavelength. For SIM imaging on fixed cells, it is possible to use mounting medium with a higher RI (i.e. RI close to that of the glass coverslips), which reduces the spherical aberrations, thus enabling larger z-stacks and a wider spectrum of colors to be imaged before artifacts from mismatched oil arise. However, for live-cell imaging, the cells are kept in a low RI buffer solution like RPMI or live-cell imaging buffer (RI ~ 1.33), which leads to additional spherical aberrations and loss of fluorescent signal at the sample-coverslip interface. Therefore, matching the RI of the immersion oil for live-cell imaging is even more critical than for fixed-cell imaging.

Because of these PSF variabilities, SIM imaging using more than one wavelength means using sub-optimal oil for at least one color. For example, in the three-color image in Figure 6, immersion oil with RI 1.516 was used, while the optimal oil RI for only Gtom (ex. $\lambda = 488$ nm) in the same sample would be approximately 1.512, and 1.518 for MT only (ex. $\lambda = 642$ nm). Although the different colors have different optimal oil RIs, well-prepared samples can often be successfully imaged using immersion oil with RI between the optimal for the longest and the shortest wavelengths. In this case, we found that using oil with RI 1.516 was most suitable to achieve the best image reconstructions for all three colors during live-cell imaging. In Supplementary Figure S6, the speckled honeycomb pattern in the green channel (Gtom shown in turquoise) is an imaging artifact likely caused by this compromise in oil RI but may also be caused in part by photobleaching.

3 Conclusions

Three distinct and spectrally separated probes were used to simultaneously label sub-mitochondrial compartments in living cells, then imaged using both DV and 3D SIM. DV enabled long-term time-lapse imaging of mitochondria (60 time points over 30 min), while 3D SIM provided details about the sub-mitochondrial morphologies at single time points.

We evaluated several mitochondrial probes and labeling protocols and observed their direct effects, both individually and combined, on mitochondrial morphology and function. While BM labeling (targeting the matrix) alone resulted in some morphological artifacts, cells first transfected with Gtom (targeting the outer membrane) and then transduced with BM showed lower incidence of these artifacts. Although lower concentrations of MT (targeting the intermembrane space) did not show morphological artifacts during single time point imaging, phototoxicity induced by extended imaging time resulted in a swollen appearance of the mitochondria. However, MT was the only probe with sufficient photostability for time-lapse 3D SIM imaging beyond five time points for our cells and labeling conditions, irrespective of the time in-between each point.

For dual-labeling experiments, the best results were obtained with Gtom and MT, such that no modification of the individual labeling protocols was required when the probes were used in combination, and no changes in morphology were noted as compared to cells labeled with the probes individually. For the other two combinations,

optimization of the labeling protocol was necessary, and morphological artifacts were observed. However, additional BM labeling of Gtom-transfected cells reduced the incidence of morphological artifacts compared to cells labeled only with BM.

In addition to reducing the suitability for 3D SIM imaging, the reduced labeling efficiency of the combined probes also serves as a reminder that altering cells with fluorescent probes necessarily changes the biological system under study. The effects of these changes, especially when combined with powerful investigative tools (e.g. imaging with high spatio-temporal resolution), may potentially lead to false interpretations and conclusions. For example, morphological artifacts from over-expression of a host protein may change from unnoticeable to especially noteworthy at SR. In addition, phototoxic effects present challenges to evaluating the dynamics of a system, as the simple act of observing a target can damage it or otherwise influence its behavior; these effects are compounded in SR microscopy, where the total light dose on the sample is significantly increased.

It is therefore important to evaluate and choose the best combination of techniques for each specific scientific inquiry. Although, on one hand, 3D SIM clearly provides higher resolution, it comes with a requirement for increased labeling, higher risks of phototoxic effects, lower imaging speed, and lower potential for time-lapse imaging. DV imaging, on the other hand, is a good choice for lower phototoxicity and higher speed compared to both SIM and confocal imaging, but it lacks the resolution of the former and is not as good for imaging thick samples as the latter. For imaging mitochondria in our study, the combination of DV for time-lapse and 3D SIM for detailed, single time-point analysis proved to be most useful. Similarly, the choice of probes is highly dependent on the goals and conditions of each experiment. MT labeling is fast, relatively bright, and photostable but prone to morphological artifacts depending on both labeling and imaging conditions. Gtom provides an excellent, distinct structure for imaging, but the requirements for transfection make it incompatible with some primary cells, and varying expression levels can make it difficult to find and image cells using 3D SIM. BM labeling is somewhat slower and more prone to artifacts, although it may still be a good choice for cells that do not tolerate MT labeling or imaging. As our study focused on MCC13 cells, the choice of labeling and imaging conditions may vary for different sample types and conditions and for the process or subject under evaluation. Our study also emphasizes the importance of and need for development of sub-cellular probes compatible with both SR microscopy and live-cell imaging.

Resolving and visualizing three different compartments of mitochondria at the same time in a living cell is an important step towards understanding the nanomachinery of the basic units of life. This work highlights the capability of current techniques to evaluate differences in nanoscale structures within a living system and the challenges involved in modifying and studying biological systems with high resolution. With current research trends emphasizing the dynamics of individual proteins or gene expression levels, the sub-organelle level of detail elucidated here will become increasingly relevant and, therefore, so will an understanding of the associated challenges and limitations of these advanced techniques.

4 Methods

4.1 Cell lines

The Merkel cell carcinoma (MCC13) cells were maintained in an incubator at 37°C with 20% O_2 and 5% CO_2, with a growth medium consisting of RPMI 1640 (Sigma-Aldrich Norway AS, Oslo, Norway) supplemented with 10% fetal bovine serum (FBS) (Sigma-Aldrich Norway AS, Oslo, Norway) and 1% penicillin/streptomycin (Sigma-Aldrich Norway AS, Oslo, Norway). Cultures used for experiments were thawed from stocks stored in liquid nitrogen a minimum of 1 week prior to transfection.

4.2 Transfection of cells using lipofectamine

Bacterial stabs for growing Gtom plasmids were obtained from Addgene (Cambridge, MA, USA) (plasmid # 54282) [43]. Selected bacterial colonies were inoculated overnight in liquid Luria-Bertani (LB) broth (Difco, Thermo Fisher Scientific, Waltham, MA, USA). Plasmid DNA (pDNA) was purified using the GeneJET Plasmid Miniprep Kit (Thermo Fisher, Waltham, MA, USA). Prior to transfection, the cells were seeded on glass-bottom culture dishes (MatTek Corporation, Ashland, MA, USA) and cultured in antibiotic-free medium until they reached 80% confluency. Transfection was performed using 1 μg purified pDNA and 1 μl Lipofectamine 3000 (Invitrogen, Thermo Fisher Scientific, Waltham, MA, USA) in Opti-MEM media for 5 h at 37°C before changing to normal growth medium without antibiotics and incubated for 2 days. The cells were then imaged or incubated further in medium containing 0.2 mg/ml Geneticin Selective Antibiotics (Thermo Fisher Scientific, Waltham, MA, USA) for selection of Gtom-expressing cells.

4.3 Labeling with CellLight Mitochondria-RFP BacMam 2.0 (BM)

Labeling with BM (Thermo Fisher Scientific, Waltham, MA, USA) was done according to manufacturer's protocol with 15–45 particles per cell (PPC) approximately 20 h prior to imaging. Transfected cells were grown under the same cell culture conditions as described above but in antibiotic-free medium.

4.4 Labeling with MitoTracker

MitoTracker labeling was optimized for MitoTracker Green (MTG) (Thermo Fisher Scientific, Waltham, MA, USA) with emphasis on TL imaging. The optimal concentration for MTG was also found suitable for MitoTracker Deep Red.

Labeling concentrations were tested in the range of 10–400 nм, with incubation times ranging from 15 to 45 min. The most suitable results (for non-BM transduced cells) were obtained with 75–100 nм MT with incubation for 30 min, followed by three washes for 10 s with 1-ml phosphate-buffered saline (PBS) or live-cell imaging medium (Thermo Fisher Scientific, Waltham, MA, USA). For MitoTracker Deep Red (Thermo Fisher Scientific, Waltham, MA, USA), an additional washing step was necessary to sufficiently reduce the background signal for optimal SIM image reconstruction. For combined experiments with BM and Gtom, MT incubation was applied as the final labeling step.

4.5 Three-color mitochondrial labeling

As described in more detail above, cells were first labeled with Gtom through lipofectamine transfection of plasmid DNA. Transfected cells were allowed to recover and then positively selected using Geneticin before further labeling. After 2 days, the Gtom-labeled cells were then transduced with BM and then incubated for an additional 16–20 h. Immediately before imaging, the cells were incubated with MT for 30 min then washed in PBS or live-cell imaging medium. The workflow is summarized below in Figure 7.

4.6 Imaging parameters

4.6.1 Microscope

Images were acquired using a DeltaVision OMX V4 Blaze imaging system (GE Healthcare Life Sciences,
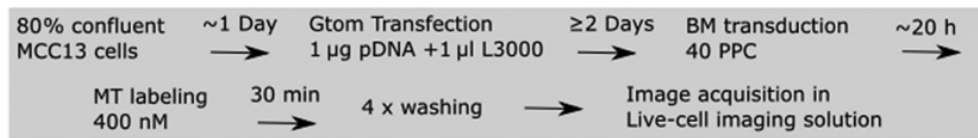
Figure 7: Flow chart summarizing the optimized protocol for three-color labeling of mitochondria.

Marlborough, MA, USA) equipped with a 60X 1.42NA oil-immersion objective (Olympus); three sCMOS cameras; and 488-, 568-, and 642-nm lasers for excitation. The vendor specified optical resolution of the system (3D SIM) is 110–160 nm laterally and 340–380 nm axially, depending on color channel. Multiple channels were imaged sequentially before stepping through z-planes. Illumination intensity, exposure time, and time-lapse period were optimized for each individual label. Supplementary Table S1 gives an overview of individual image parameters.

4.6.2 Image processing

Deconvolution and 3D SIM image reconstruction were completed using the manufacturer-supplied SoftWoRx program (GE Healthcare Life Sciences, Marlborough, MA, USA). Image registration (color alignment) was also performed in SoftWoRx using experimentally measured calibration values compensating for minor lateral and axial shifts, rotation, and magnification differences between cameras. Further image processing was done using Fiji [44], and 3D movies were generated using Volocity version 6.3 (Perkin Elmer, Waltham, MA, USA).

Author contributions statements: B.S.A. and D.L.W conceived and supervised the project. I.S.O., B.S.A., and D.L.W designed the research. I.S.O. performed all the experiments on microscopy and D.L.W. assisted during the experiments. I.S.O and C.I.Ø. prepared and stained the cells. I.S.O. reconstructed the images, analyzed the data, and prepared the figures. All authors contributed in writing the manuscript.

Competing financial interests: The authors declare no competing financial interests.

References

[1] Nunnari J, Suomalainen A. Mitochondria: in sickness and in health. Cell 2012;148:1145–59.

[2] Jakobs S, Wurm CA. Super-resolution microscopy of mitochondria. Curr Opin Chem Biol 2014;20:9–15.

[3] Mitra K, Lippincott-Schwartz J. Analysis of mitochondrial dynamics and functions using imaging approaches. Curr Protoc Cell Biol 2010; Chapter 4: Unit 4.25.1–21. doi:10.1002/0471143030.cb0425s46.

[4] York AG, Chandris P, Nogare DD, et al. Instant super-resolution imaging in live cells and embryos via analog image processing. Nat Meth 2013;10:1122–6.

[5] Takihara Y, Inatani M, Eto K, et al. In vivo imaging of axonal transport of mitochondria in the diseased and aged mammalian CNS. Proc Natl Acad Sci 2015;112:10515–20.

[6] Xu Y, Chen M, Hu B, Huang R, Hu B. In vivo imaging of mitochondrial transport in single-axon regeneration of zebrafish Mauthner cells. Front Cell Neurosci 2017;11:4.

[7] Monteith A, Marszalec W, Chan P, et al. Imaging of mitochondrial and non-mitochondrial responses in cultured rat hippocampal neurons exposed to micromolar concentrations of TMRM. PLoS One 2013;8:e58059.

[8] Goldenthal MJ. Mitochondrial involvement in myocyte death and heart failure. Heart Fail Rev 2016;21:137–55.

[9] Murphy E, Ardehali H, Balaban RS, et al. Mitochondrial function, biology, and role in disease: a scientific statement from the american heart association. Circ Res 2016;118:1960–91.

[10] O'Rourke B. Metabolism: beyond the power of mitochondria. Nat Rev Cardiol 2016;13:386–8.

[11] Wai T, Langer T. Mitochondrial dynamics and metabolic regulation. Trends Endocrinol Metab 2016;27:105–17.

[12] Scaduto RC Jr, Grotyohann LW. Measurement of mitochondrial membrane potential using fluorescent rhodamine derivatives. Biophys J 1999;76:469–77.

[13] Detmer SA, Chan DC. Functions and dysfunctions of mitochondrial dynamics. Nat Rev Mol Cell Biol 2007;8:870–9.

[14] Galbraith CG, Galbraith JA. Super-resolution microscopy at a glance. J Cell Sci 2011;124:1607–11.

[15] Schermelleh L, Heintzmann R, Leonhardt H. A guide to super-resolution fluorescence microscopy. J Cell Biol 2010;190:165–75.

[16] Waldchen S, Lehmann J, Klein T, van de Linde S, Sauer M. Light-induced cell damage in live-cell super-resolution microscopy. Sci Rep 2015;5:15348.

[17] Gustafsson MG, Shao L, Carlton PM, et al. Three-dimensional resolution doubling in wide-field fluorescence microscopy by structured illumination. Biophys J 2008;94:4957–70.

[18] Schermelleh L, Carlton PM, Haase S, et al. Subdiffraction multicolor imaging of the nuclear periphery with 3D structured illumination microscopy. Science 2008;320:1332–6.

[19] Hirano Y, Matsuda A, Hiraoka Y. Recent advancements in structured-illumination microscopy toward live-cell imaging. Microscopy (Oxf) 2015;64:237–49.

[20] Mönkemöller V, Øie C, Hübner W, Huser T, McCourt P. Multimodal super-resolution optical microscopy visualizes the close connection between membrane and the cytoskeleton in liver sinusoidal endothelial cell fenestrations. Sci Rep 2015;5:16279.

[21] Dempsey GT, Vaughan JC, Chen KH, Bates M, Zhuang X. Evaluation of fluorophores for optimal performance in localization-based super-resolution imaging. Nat Methods 2011;8:1027–36.

[22] Agarwal K, Macháň R. Multiple signal classification algorithm for super-resolution fluorescence microscopy. Nat Commun 2016;7:13752.

[23] Szczurek A, Klewes L, Xing J, et al. Imaging chromatin nanostructure with binding-activated localization microscopy based on DNA structure fluctuations. Nucleic Acids Res 2017;45:e56.

[24] Perry AJ, Rimmer KA, Mertens HD, et al. Structure, topology and function of the translocase of the outer membrane of mitochondria. Plant Physiol Biochem 2008;46:265–74.

[25] Chacinska A, Koehler CM, Milenkovic D, Lithgow T, Pfanner N. Importing mitochondrial proteins: machineries and mechanisms. Cell 2009;138:628–44.

[26] Thermo Fisher Scientific. Description of 'CellLight Mitochondria-RFP, BacMam 2.0'. Available at: https://www.thermofisher.com/order/catalog/product/C10505.

[27] Melkko J, Hellevik T, Risteli L, Risteli J, Smedsrod B. Clearance of NH2-terminal propeptides of types I and III procollagen is a physiological function of the scavenger receptor in liver endothelial cells. J Exp Med 1994;179:405–12.

[28] Di Maio R, Barrett PJ, Hoffman EK, et al. α-Synuclein binds to TOM20 and inhibits mitochondrial protein import in Parkinson's disease. Sci Transl Med 2016;8:342ra78.

[29] Kholmukhamedov A, Schwartz JM, Lemasters JJ. MitoTracker probes and mitochondrial membrane potential. Shock (Augusta, Ga.) 2013;39:543.

[30] Lemasters JJ. Modulation of mitochondrial membrane permeability in pathogenesis, autophagy and control of metabolism. J Gastroenterol Hepatol 2007;22:S31–7.

[31] Genetics Home Reference. *PDHA1 gene*. Available at: http://ghr.nlm.nih.gov/gene/PDHA1.

[32] Genetics Home Reference. Pyruvate dehydrogenase deficiency. https://ghr.nlm.nih.gov/condition/pyruvate-dehydrogenase-deficiency.

[33] Burte F, Carelli V, Chinnery PF, Yu-Wai-Man P. Disturbed mitochondrial dynamics and neurodegenerative disorders. Nat Rev Neurol 2015;11:11–24.

[34] Wang X, Gerdes HH. Transfer of mitochondria via tunneling nanotubes rescues apoptotic PC12 cells. Cell Death Differ 2015;22:1181–91.

[35] Sanchez V, Villalba N, Fiore L, et al. Characterization of tunneling nanotubes in Wharton's jelly mesenchymal stem cells. An Intercellular exchange of components between neighboring cells. Stem Cell Rev Rep 2017;13:1–8.

[36] Pasquier J, Guerrouahen BS, Al Thawadi H, et al. Preferential transfer of mitochondria from endothelial to cancer cells through tunneling nanotubes modulates chemoresistance. J Transl Med 2013;11:94.

[37] Torralba D, Baixauli F, Sánchez-Madrid F. Mitochondria know no boundaries: mechanisms and functions of intercellular mitochondrial transfer. Front Cell Dev Biol 2016;4:107.

[38] Berridge MV, McConnell MJ, Grasso C, Bajzikova M, Kovarova J, Neuzil J. Horizontal transfer of mitochondria between mammalian cells: beyond co-culture approaches. Curr Opin Genet Dev 2016;38:75–82.

[39] Pouli D, Balu M, Alonzo CA, et al. Imaging mitochondrial dynamics in human skin reveals depth-dependent hypoxia and malignant potential for diagnosis. Sci Transl Med 2016;8:367ra169.

[40] Shao L, Kner P, Rego EH, Gustafsson MG. Super-resolution 3D microscopy of live whole cells using structured illumination. Nat Methods 2011;8:1044–6.

[41] Icha J, Weber M, Waters CJ, Norden C. Phototoxicity in live fluorescence microscopy, and how to avoid it. Bioessays 2017;39:1700003.

[42] Magidson V, Khodjakov A. Circumventing photodamage in live-cell microscopy. Methods Cell Biol 2013;114:545–60.

[43] Addgene. mEmerald-TOMM20-N-10. Available at: www.addgene.org/54282/.

[44] Schindelin J, Arganda-Carreras I, Frise E, et al. Fiji: an open-source platform for biological-image analysis. Nat Methods 2012;9:676–82.